Applied Catalysis B: Environmental 340 (2024) 123216

Contents lists available at ScienceDirect

Applied Catalysis B: Environmental

journal homepage: www.elsevier.com/locate/apcatb

Linkage engineering in covalent organic frameworks as metal-free oxygen reduction electrocatalysts for hydrogen peroxide production

Shaoda Huang [a,b], Bingyan Zhang [a], Dongshuang Wu [b], Yifan Xu [b], Hongyin Hu [a], Fang Duan [a], Han Zhu [a], Mingliang Du [a], Shuanglong Lu [a,*]

[a] Key Laboratory of Synthetic and Biological Colloids, Ministry of Education, School of Chemical and Material Engineering, Jiangnan University, Wuxi, Jiangsu 214122, PR China

[b] School of Materials Science and Engineering, Natural Sciences and Science Education in National Institute of Education, Nanyang Technological University, Singapore 637616, Singapore

ARTICLE INFO

Keywords:
Covalent organic frameworks
2e$^-$ oxygen reduction reaction
Linkage
Electrocatalysts
Hydrogen peroxide

ABSTRACT

Covalent organic frameworks (COFs) are promising platforms with tailorable structures toward metal-free electrocatalytic oxygen reduction (ORR). Here, COFs with different linkages were constructed and explored in the selective two-electron ORR (2e$^-$ ORR) for hydrogen peroxide (H_2O_2) production. Interestingly, imine-linked Py-TD-COF delivers a remarkable H_2O_2 selectivity of 80–92 %, while amine-linked Py-TD-COF-NH exhibits relatively low H_2O_2 selectivity of 50–61 %. Experimental and theoretical results reveal that the donor-accepter property of Py-TD-COF enables proper activation of O_2, while Py-TD-COF-NH shows relatively high activation of O_2 due to the electronic modulation induced by the linkage transformation. Furthermore, the potential H-bonding between the amine group and the adsorbed oxygen molecules on Py-TD-COF-NH is proved to elongate the O—O bond, thus accelerating the subsequent hydrogenation and lowering the barrier for the reduction of *OOH to *O intermediates. This work highlights the importance of suitable linkages and provides a guideline for designing metal-free COF catalysts for 2e$^-$ ORR.

1. Introduction

Hydrogen peroxide (H_2O_2) is one of the most important chemicals in industry, with versatile applications in various fields such as wastewater treatment, textile bleaching, chemical synthesis, and so on [1–4]. The global demand for H_2O_2 is dramatically growing and will reach 6000 kilotons by 2024 [5,6]. Until now, the H_2O_2 production still depends heavily on the anthraquinone process. It is well known that this process causes huge environmental pollution and energy consumption [7–9]. Therefore, there is an urgent need to develop environment-friendly and high-efficient H_2O_2 production routes. Recently, the electrochemical oxygen reduction reaction (ORR) based on the two-electron (2e$^-$) pathway is considered a promising approach to generate H_2O_2 in the ambient environment. However, the competitive four-electron (4e$^-$) pathway in the ORR process could severely impede the 2e- pathway, thus diminishing the efficiency of H_2O_2 production [10–14]. At present, various metal electrocatalysts, including noble metal and transition metal-based electrocatalysts, have shown high efficiency for 2e$^-$ ORR [15–20]. However, the scarcity and easily-poisoning of these catalysts hinder their widespread utilization. In this regard, it is of great significance to design and develop metal-free electrocatalysts with a high tendency toward 2e$^-$ ORR for H_2O_2 synthesis.

Covalent organic frameworks (COFs) are a recently emerging class of highly ordered porous organic polymers with striking features such as pre-designable structures, controllable synthesis, and manageable functions [21–27]. Therefore, the well-defined structures and precise active sites can be designed in their frameworks in advance, meeting the requirements for advanced electrocatalysis in various electrochemical applications [28–31]. For example, Long and coworkers reported metal-free carbon-based COFs for the efficient 4e$^-$ oxygen reduction to H_2O [32]. It is unclosed that the enhancement of catalytic activity should be attributed to the effective regulation of the molecular configuration and charge redistribution, as well as the improvement of charge transfer. Similarly, it is well revealed that the critical knob for the 2e$^-$ electrochemical reduction of oxygen to H_2O_2 heavily depends on the thermodynamic adsorption behaviors of main intermediates on catalytically active sites, which could also be regulated by their electronic structures. In our recent work, the elaborate thiophene-based COFs have

* Corresponding author.
E-mail address: lushuanglong@jiangnan.edu.cn (S. Lu).

https://doi.org/10.1016/j.apcatb.2023.123216
Received 16 June 2023; Received in revised form 9 August 2023; Accepted 22 August 2023
Available online 23 August 2023

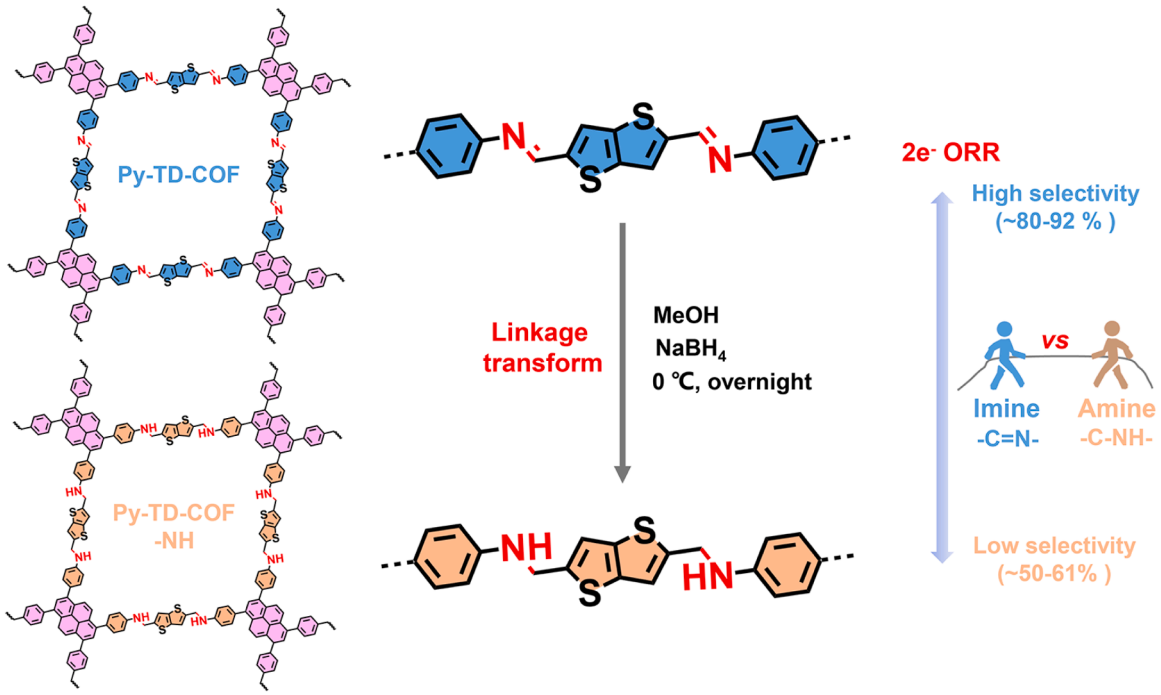

Fig. 1. The chemical structures of Py-TD-COF, Py-TD-COF-NH, and the schematic illustration of their electrocatalytic 2e⁻ ORR.

been demonstrated to be efficient electrocatalysts for 2e⁻ ORR [33]. The 2e⁻ ORR selectivity and activity could be flexibly regulated by matching proper building blocks. The interesting results revealed that the electronic environment of active sites could be optimized to tune the adsorption behaviors of oxygen and intermediates. This provides an important concept for designing ideal metal-free COF catalysts toward 2e⁻ ORR. Apart from building blocks, recent research demonstrated that suitable linkages could also effectively optimize the electronic structure of COFs [34–36]. As an example, Zhao et al. found that ketoenamine-linked COFs exhibited a more favorable electronic structure than imine-linked COFs for photocatalytic hydrogen evolution [37]. In addition, the suitable linkage could provide a favorable chemical interaction to facilitate electrocatalytic reductions [34,38,39]. For instance, Fang et al. developed a class of ladder-type polyaniline-analogous COFs by converting imine linkages (-C═N-) into amine linkages (-C-NH-) [38]. They displayed excellent performance toward electrocatalytic CO_2 reduction. It is proposed that an amine-linked framework could offer specific chemical surroundings for the favorable chemisorption of CO_2 molecules, thus improving the electrocatalytic activity. Apparently, linkage engineering has been confirmed to be an efficient strategy to tailor the catalytic behaviors of COFs. It is meaningful to illustrate the influence of linkages in COFs on the 2e⁻ ORR performance, as well as to get an insight into their inherent mechanisms.

Herein, a typical imine-linked COF (Py-TD-COF, Py: tetrakis(4-aminophenyl)pyrene, TD: thieno[3,2-*b*]thiophene-2,5-dicarbaldehyde) was constructed, and correspondingly, the amine-linked COF (Py-TD-COF-NH) was synthesized by a facile direct reduction. Their electrocatalytic 2e⁻ ORR performance was systematically explored. Interestingly, Py-TD-COF with donor-accepter property shows a remarkable H_2O_2 selectivity of 80–92 % in the potential range of 0.2–0.7 V vs. RHE, while Py-TD-COF-NH exhibits relatively low H_2O_2 selectivity of 50–61 % at the same potential wide. The experimental results and theoretical calculation revealed that Py-TD-COF and Py-TD-COF-NH have different electronic structures, which lead to the change in the adsorption ability of oxygen molecules on active sites. Moreover, the optimized structure of the COF–O_2 (COF–OOH) species shows that the O—O bond in Py-TD-COF-NH is elongated to 1.36 Å relative to 1.25 Å in Py-TD-COF. Directed H-bonding in amine linkage holds the key factor to this elongation as well as the weakening of the O—O bond. The elongated O—O bond could facilitate the subsequent hydrogenation step, which is evidenced by the more downhill in free energy for *OOH reduction to *O on Py-TD-COF-NH. Moreover, the barrier for *OOH dissociation to *OH on Py-TD-COF-NH is much reduced, and the ΔG_{*O}-ΔG_{H2O2} on the Py-TD-COF-NH is relatively higher than that of Py-TD-COF. It is proposed that the relatively stronger activation of O_2 and potential H-bonding in amine linkage are responsible for the diminishment of H_2O_2 selectivity in Py-TD-COF-NH. This work well reveals the intrinsic correlation between linkages of COFs and electrocatalytic ORR behavior, which provides a guideline to design metal-free COFs materials by linkage engineering for electrochemical applications.

2. Experimental

Detailed information regarding the chemicals and instrumentation can be found in the Supporting information accompanying this study.

2.1. Synthesis of Py-TD COF and Py-TD-COF-NH

The Py-TD COF was synthesized via a modified solvothermal method based on the Schiff base reaction [40]. Specifically, 14 mg of Py (0.02 mmol) and 7.9 mg of TD (0.04 mmol) were combined in a Pyrex tube with a solvent mixture of mesitylene/benzyl alcohol (1 mL, 2:1, v/v) and 6 M acetic acid (100 μL). The resulting mixture was sonicated to achieve a homogeneous solution and subjected to freeze-pump-thaw cycles three times to degas. The mixture was subsequently heated to 120 ℃ for 3 days in an oven. After cooling to room temperature, the sample was collected via centrifugation, washed several times with tetrahydrofuran and ethanol, and further activated by Soxhlet extraction with tetrahydrofuran for 12 h. Finally, the product was dried under vacuum at 60 °C for 12 h to obtain the final product.

The Py-TD-COF-NH was synthesized via a one-step reduction method. Firstly, 23.0 mg of p-phthalic acid was added to a suspension of 20.0 mg of Py-TD COF in 25 mL of methanol (MeOH). The mixture was stirred in an ice bath for 5 min before adding a $NaBH_4$ solution (20 mmol/5 mL). After stirring for 1 h, the mixture was transferred and

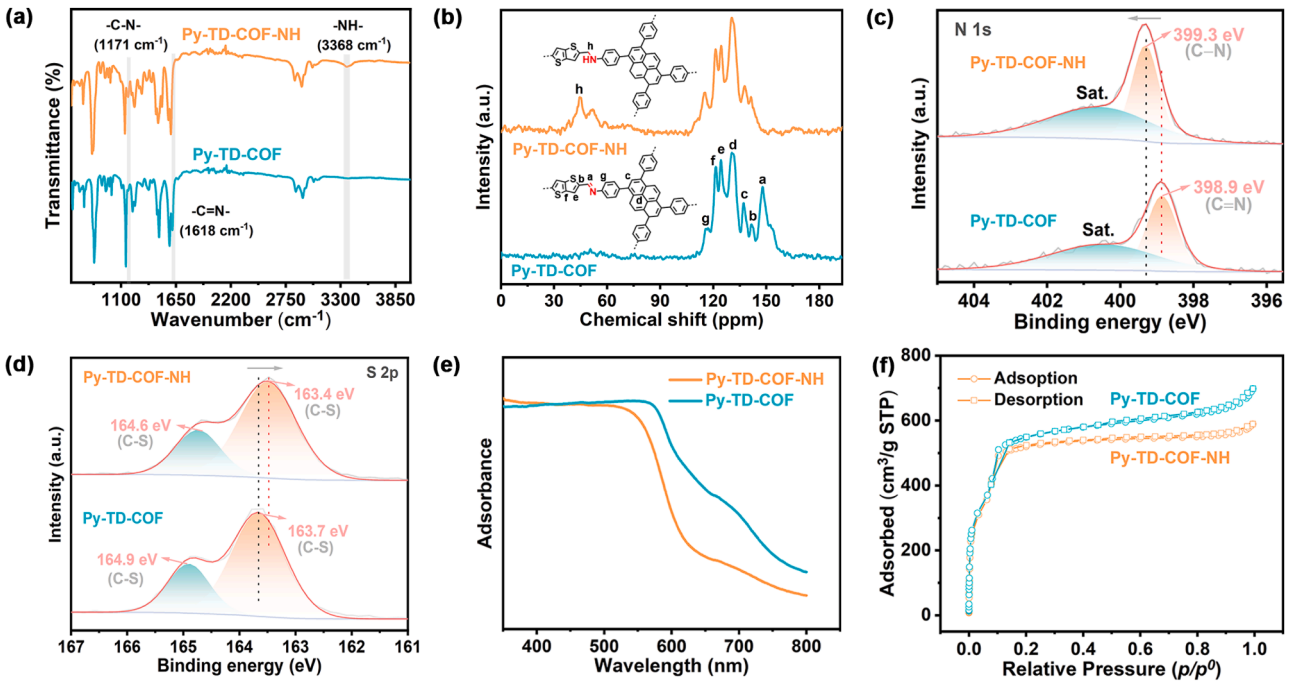

Fig. 2. (a) FT-IR spectra, (b) Solid-state ^{13}C NMR spectra, (c) the N1s XPS spectra, (d) the S2p XPS spectra, (e) UV-Vis diffuse reflectance spectra, (f) N_2 isotherms plots at 77 K of Py-TD-COF-NH and Py-TD-COF.

stirred at room temperature overnight. Finally, the product was collected by centrifugation and washed with methanol three times. This obtained product was dried under vacuum at 60 °C for 12 h.

3. Result and discussion

3.1. Synthesis and characterizations of COFs

Py-TD-COF with imine linkage was prepared through the typical Schiff base reaction using TD and Py as building blocks [40]. The TD units, with redox-active ability, are proved to be active sites toward ORR, while the Py units, with electron-rich skeleton, serve as typical electron donors to regulate the behavior of oxygen adsorption on TD [41]. Afterward, Py-TD-COF-NH with amine linkage was synthesized by the direct reduction of the corresponding Py-TD-COF (Fig. 1, See the Experimental for the detailed synthesis).

The chemical structures of synthesized Py-TD-COF and Py-TD-COF-NH were first characterized by Fourier transform infrared (FT-IR) spectroscopy. For Py-TD-COF, it is clearly seen that the peak at around 1618 cm^{-1} (-C═N-) appears, while the peaks at 1656 cm^{-1} (C═O band for TD) and 1285 cm^{-1} (-NH_2 band for Py) disappear (Fig. 2a and Fig. S1). These pieces of evidence confirm that the monomers were successfully transferred and linked by imine groups. For comparison, a fresh peak at 1171 cm^{-1} corresponding to -C-N- vibration stretch is observed for Py-TD-COF-NH (Fig. 2a), demonstrating the conversion of -C═N- to -C-N- after the reduction [36]. To further validate the quantitative conversion of imine to amine linkages, the ^{13}C cross-polarization solid-state nuclear magnetic resonance (^{13}C NMR) spectrum was performed. As shown in Fig. 2b, Py-TD-COF presents a typical carbon peak in imine (-C═N-) at 148.4 ppm, which is not detected for Py-TD-COF-NH. Correspondingly, a new peak at 44.5 ppm, indexed as carbon in amine (-C-NH-), is observed for Py-TD-COF-NH. X-ray photoelectron spectroscopy (XPS) was then conducted to reveal the definite chemical structure and composition of COFs. To be specific, the C 1s peak of Py-TD-COF exhibits three split peaks at binding energies of 284.7 eV, 285.1 eV, and 285.9 eV, assigning to the sp^2 C═C, C═N/C-N, and C-S bonds, respectively (Fig. S2). The C 1s peak of Py-TD-COF-NH shows similar split peaks at 284.8 eV, 285.1 eV, and 285.8 eV (Fig. S2). Noticeably, after reduction, higher binding energy for the N 1s in Py-TD-COF-NH (399.3 eV) is found when compared with their corresponding imine frameworks (398.9 eV), which further reflects the chemical conversion of the original -C═N- bonds (Fig. 2c). As an indicator of the active sites' electronic structures in the COFs, the S 2p spectra of thiophene units in Py-TD-COF and Py-TD-COF-NH were further collected and shown in Fig. 2d. A negative shift is found for the typical peaks of S $2p_{3/2}$ and S $2p_{1/2}$ in COFs after the reduction, from 163.7 eV and 164.9 eV in Py-TD-COF to 163.4 eV and 164.6 eV in Py-TD-COF-NH. It illustrates the remote electronic modulation on the active sites through the linkage transformation. The electronic structures of Py-TD-COF and Py-TD-COF-NH were further evaluated by UV–vis absorption. The Py-TD-COF has a smaller band gap of 1.95 eV than that of Py-TD-COF-NH (2.01 eV), showing red-shift adsorption compared to Py-TD-COF-NH (Fig. 2e and Fig. S3). The TGA analysis indicated that Py-TD-COF and Py-TD-COF-NH have desirable thermal stability with thermal decomposition temperatures over 425 ℃ (Fig. S4). The specific surface areas of Py-TD-COF and Py-TD-COF-NH were analyzed by nitrogen adsorption tests at 77 K. Brunauer–Emmett–Teller (BET) surface area of Py-TD-COF is determined to be 1726 m^2/g, which is highly close to that of Py-TD-COF-NH (1713 m^2/g) (Fig. 2f and Fig. S5). It demonstrates the reduction process on the imine linkage doesn't influence the porous properties of produced amine-linked COFs.

Powder X-ray diffraction (PXRD) patterns were then performed to analyze the crystallinities of Py-TD-COF-NH and Py-TD-COF. The intensive diffraction peaks at around 3.6°, 5.0°, 7.1°, 10.6°, 14.5°, and 24.3°, corresponding to the (110), (200), (220), (330), (440), and (001) planes, are both indexed in the experimental PXRD patterns of Py-TD-COF-NH and Py-TD-COF, respectively (Fig. 3a). Computational simulation and Pawley refinement were used to rebuild the optimized theoretical structures (Fig. 3b–c). The result reveals the optimized unit cell parameters (a = 35.466751 Å, b = 34.672073 Å, c = 3.741179 Å, α = 90°, β = 75°, γ = 90°), which belongs to *C2/ M* space group. Additionally, the Pawley-refined PXRD patterns match well with the experimental data, as confirmed by the small residual values of

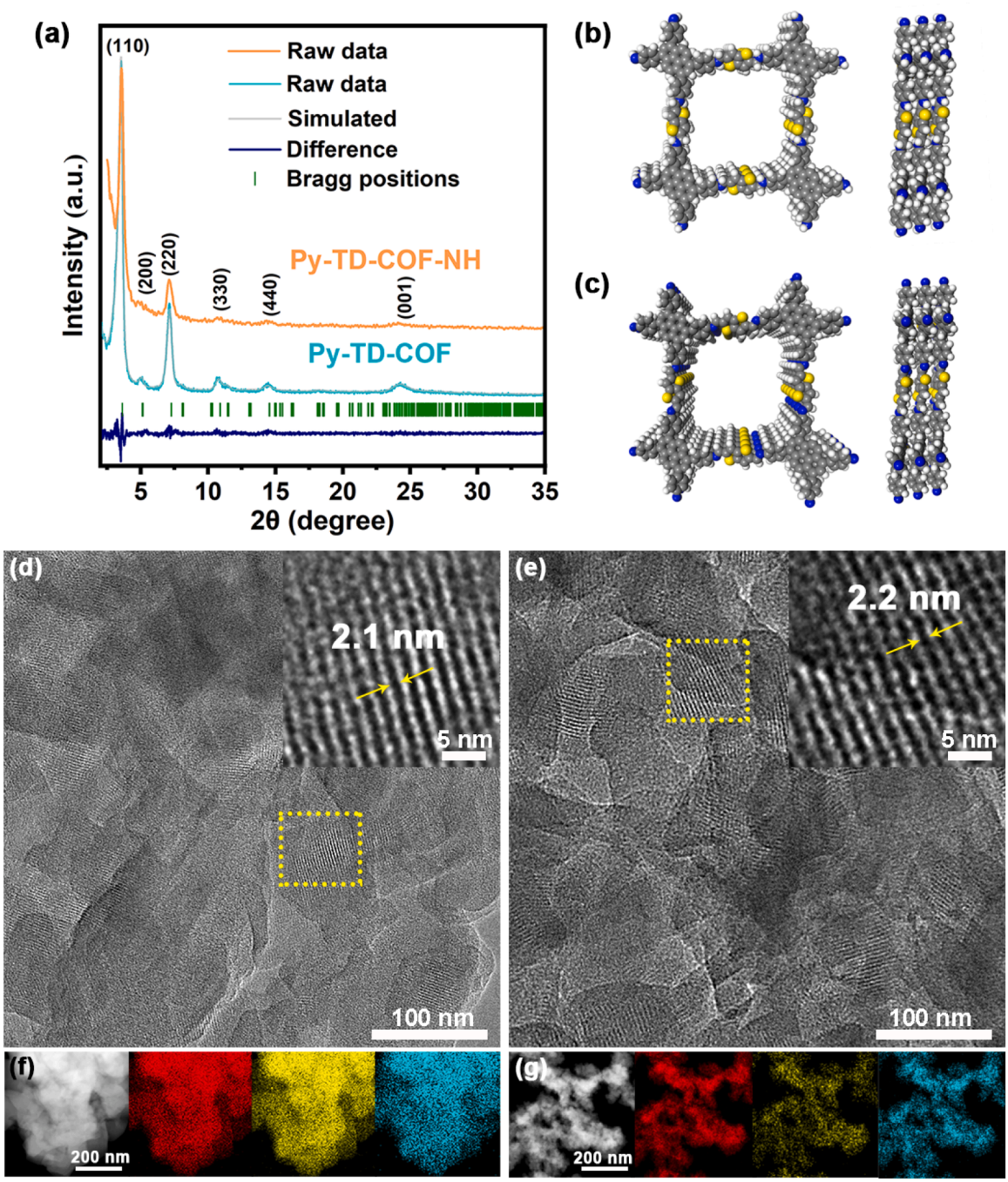

Fig. 3. (a) The experimental and simulated PXRD patterns of Py-TD-COF-NH and Py-TD-COF, (b, c) corresponding structural model, (d, e) TEM images, and (f, g) corresponding element mapping Py-TD-COF-NH and Py-TD-COF (red: C, yellow: N, cyan: S).

Rp = 4.62 % and Rwp = 3.57 %. Moreover, it is worth noticing that the peaks of Py-TD-COF-NH all show a positive shift compared to Py-TD-COF (Fig. S6), which may be related to the shorter length of the linking units and flexibility of the -C—N- bond [42]. The scanning electron microscopy (SEM) and transmission electron microscopy (TEM) images uncover that both COFs have relatively regular structured morphologies (Fig. 3d–e, Fig. S7 and S8). Moreover, the good crystallinities of Py-TD-COF and Py-TD-COF-NH are clearly revealed by HR-TEM and corresponding fast Fourier transform (FFT) patterns (Fig. S9). The crystal lattice is observed on Py-TD-COF-NH, and the corresponding lattice spacing is 2.1 nm, which can be assigned to (110) crystal planes (Inset in Fig. 3d). This value is a little bit smaller than that of Py-TD-COF (2.2 nm) (Inset in Fig. 3e), which is coincident with the PXRD results. Moreover, the corresponding element mapping results reveal the main composited elements, C, N, and S are evenly distributed in both COF samples (Fig. 3f–g). Additionally, the PXRD patterns of Py-TD-COF and Py-TD-COF-NH are still well maintained after soaking in 1 M KOH solution, indicating their outstanding chemical stability in alkaline conditions (Fig. S10).

3.2. *Electrocatalytic 2e⁻ ORR performance of COFs*

To investigate the electrocatalytic ORR performance of freshly prepared COFs in alkaline conditions, the typical three-electrode system with rotating ring-disk electrode (RRDE) equipment was used with a collect efficiency of 0.37 (Fig. S11). Firstly, Py-TD-COF and Py-TD-COF-

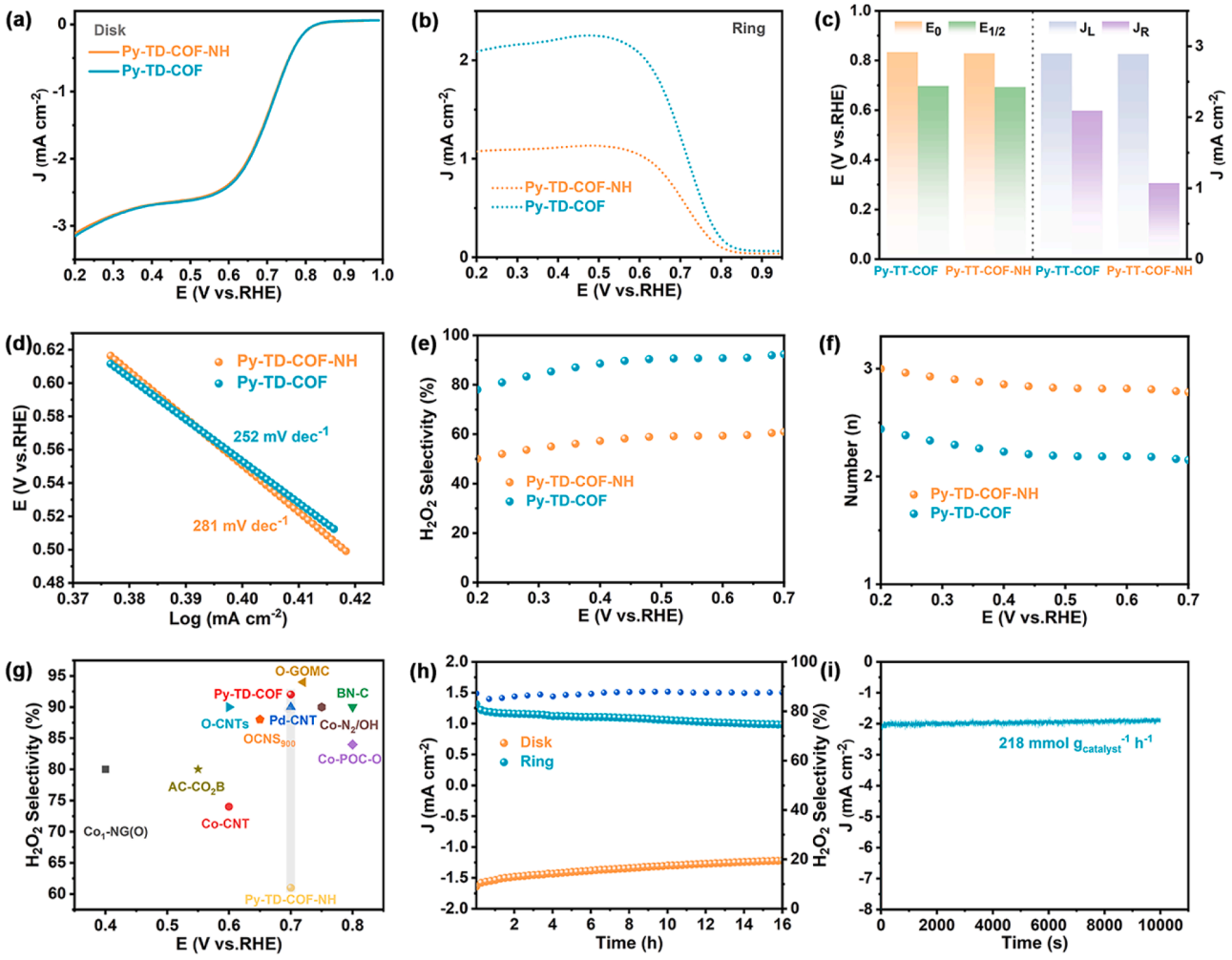

Fig. 4. (a) LSV plots collected on disk electrode, (b) LSV plots collected on ring electrode, (c) E_0, $E_{1/2}$, J_L, and J_R. (d) the Tafel plot, (e) the H_2O_2 selectivity, (f) the electron-transfer number of Py-TD-COF-NH and Py-TD-COF, (g) comparison of the H_2O_2 selectivity with recently reported catalysts, (h) durability test for Py-TD-COF, (i) *i–t* plot of the H_2O_2 generation.

NH show an intensive reduction peak from collected cyclic voltammetry (CV) plots in the O_2-saturated electrolyte, indicating they are active toward oxygen reduction (Fig. S12). The linear sweep voltammetry (LSV) plots were collected in O_2-saturated 0.1 M KOH electrolyte with a sweep rate of 10 mV s^{-1}. As shown in Fig. 4a, the collected LSV plots on the disk electrode for Py-TD-COF and Py-TD-COF-NH only show subtle differences in onset potential (E_0), half-wave potential ($E_{1/2}$), and diffusion-limited current density (J_L). Specifically, Py-TD-COF and Py-TD-COF-NH have E_0 of 0.834 and 0.829 V vs. RHE, $E_{1/2}$ of 0.698 and 0.693 V vs. RHE, and J_L of 2.898 and 2.891 mA cm^{-2}, respectively (Fig. 4a and c). It is observed that the E_0 for H_2O_2 production exceeds the thermodynamic equilibrium potential, which might be attributed to either a Nernst-related potential shift or a pH-related effect at high local alkalinity [43,44]. Interestingly, there are remarkable differences in ring current densities (J_R) on Py-TD-COF (2.093 mA cm^{-2}) and Py-TD-COF-NH (1.071 mA cm^{-2}) at 0.2 V vs. RHE (Fig. 4b and c). These results reveal the disparate selectivity of H_2O_2 on Py-TD-COF and Py-TD-COF-NH. Fig. 4d shows Tafel plots derived from the LSV curves collected on the disk electrode. The Py-TD-COF has a lower Tafel slope of 252 mV dec^{-1} than that of Py-TD-COF-NH (281 mV dec^{-1}), proving Py-TD-COF has a faster kinetic during the ORR process. The calculated H_2O_2 selectivity and electron-transfer number (n) ascertained from ring and disk current are also shown in Fig. 4e and f as a function of potentials. The Py-TD-COF has an H_2O_2 selectivity of 80–92 %, and n is determined to be ranged from 2.5 to 2.2 in a wide potential range of 0.2–0.7 V vs. RHE, demonstrating its primary $2e^-$ pathway during the ORR process. However, the H_2O_2 selectivity of Py-TD-COF-NH is calculated to be only 50–61 %, and the n is 2.8–3.0. Additionally, the Nyquist plots of Py-TD-COF and Py-TD-COF-NH were obtained and shown in Fig S13. Apparently, Py-TD-COF shows smaller charge transfer resistances than that of Py-TD-COF-NH. These results indicate that the linkage changes from imine to amine significantly induce the COF's disparate electrochemical performance during ORR process. Noticeably, the high H_2O_2 selectivity of Py-TD-COF is superior to most previously reported metal-free H_2O_2 electrocatalysts in alkaline conditions, even surpassing some metal electrocatalysts (Fig. 4g and Table S1). The long-term stability of Py-TD-COF was further evaluated by the chronoamperometric test at a continuous disk potential of 0.55 V vs. RHE. It can be seen that the ring and disk density present negligible fluctuation during the constant 16 h operation. The H_2O_2 selectivity maintains at around 88 %, and the n keeps at around 2.3 (Fig. 4h and Fig. S14). Moreover, the chemical structure of Py-TD-COF shows acceptable changes after the durability test (Fig. S15–16 and S18). Obviously, Py-TD-COF possesses excellent activity and stability toward $2e^-$ ORR. Meanwhile, it is worth noting that Py-TD-COF-NH also has good structural stability during ORR process (Fig. S17-18). In view of the superior electrochemical activity and stability of Py-TD-COF toward $2e^-$ ORR, the cumulative experiment for the H_2O_2 production was conducted in an H-cell electrolyzer. The concentration of H_2O_2 was calculated to be 218 mmol $g_{catalyst}^{-1}$ h^{-1} using the cerium sulfate titration method (Fig. 4i

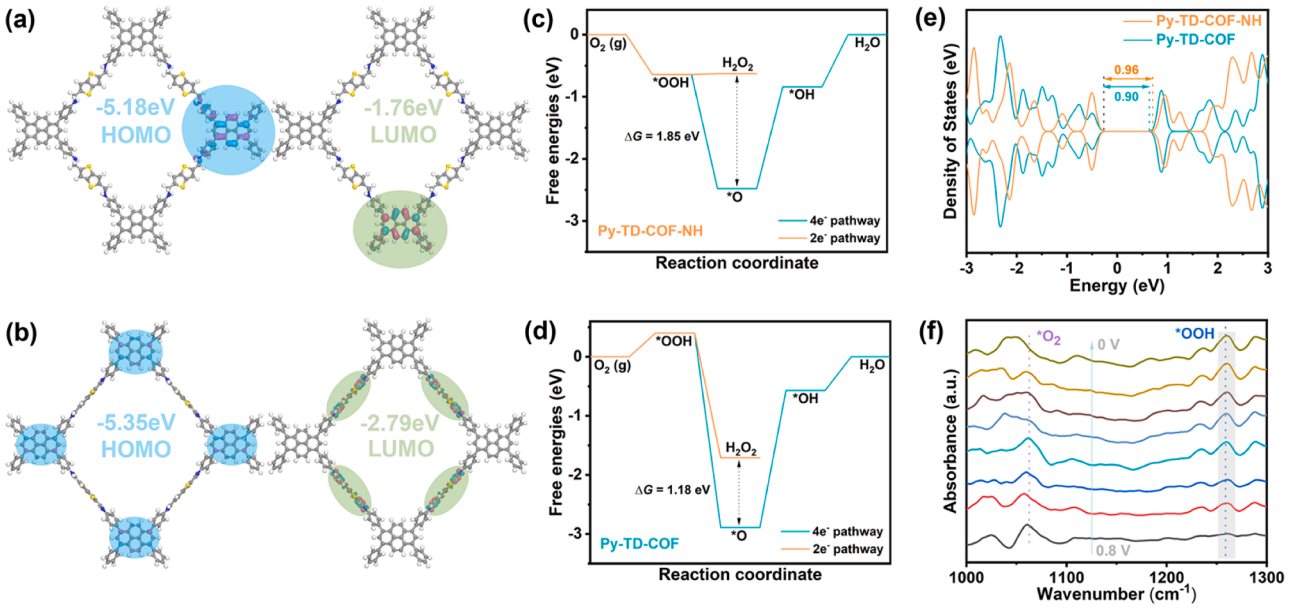

Fig. 5. LUMO and HOMO of model compounds of (a) Py-TD-COF-NH and (b) Py-TD-COF, free energy diagrams of (c) Py-TD-COF-NH and (d) Py-TD-COF, (e) DOS of Py-TD-COF-NH and Py-TD-COF, (f) Operando FTIR spectra of Py-TD-COF.

and Fig. S19). Expectedly, the generated H_2O_2 solution can be used to effectively degrade typical organic pollutants (methylene blue (MB) and Methyl orange (MO)) in wastewater through the Fenton reaction (Fig. S20, see the Supporting information for the detailed experimental description and discussion).

3.3. Theoretical calculation and operando analysis

To get a clear understanding of the main contributor to the differences in electrochemical performance of Py-TD-COF and Py-TD-COF-NH during the ORR process, density functional theory (DFT) calculations and the Vienna ab initio simulation package (VASP) were conducted based on the optimized model molecular units [45–48]. The lowest unoccupied molecular orbital (LUMO) and highest occupied molecular orbital (HOMO) of the monomers and as-prepared COFs were first calculated (Fig. S21). The LUMO-HOMO level of monomers, Py and TD, are − 1.84 eV/− 4.94 eV and − 2.93 eV/6.67 eV, respectively, implying that the electrons may transfer from Py to TD during the electrochemical reaction process. For Py-TD-COF-NH, the LUMO and HOMO are locally delocalized on Py units, with a LUMO-HOMO band gap of 3.42 eV. However, for Py-TD-COF, the LUMO is localized on the Py unit core, whereas the HOMO is on TD units, with a LUMO-HOMO band gap of 2.56 eV (Fig. 5a and b). These obvious differences between LUMO-HOMO directly uncover the distinct surface electronic properties of Py-TD-COF and Py-TD-COF-NH. Furthermore, the density of states (DOS) further illustrates that Py-TD-COF (0.90 eV) delivers a smaller band gap around the Fermi level than Py-TD-COF-NH (0.96 eV, Fig. 5e and Fig. S22), indicating their different semiconductor properties. Combined with the XPS result and UV–vis absorption, the electronic structure of Py-TD-COF-NH has been altered compared to the original Py-TD-COF due to the linkage transformation from imine to amine group. As proved in our previous research, the electronic modulation of the active sites may lead to the change in the adsorption ability of oxygen molecules, delivering different ORR behaviors [33]. To further illustrate the influences of linkage on the electrocatalytic ORR, the ORR process on Py-TD-COF and Py-TD-COF-NH for producing H_2O_2 or H_2O along a $2e^-$ or $4e^-$ pathway was investigated by DFT calculations using a computational hydrogen electrode model. It is revealed that typical intermediates, *OOH, *O, and *OH, are energetically favored to adsorb on different carbon atoms, and the most stable configurations are shown in Fig. S23–26. Firstly, possible sites around the thiophene-S structure were selected to calculate Gibbs free energy (Fig. 5c and d, Fig. S27–31). The binding energies of O_2 on the most stable active sites (site 1) of Py-TD-COF and Py-TD-COF-NH are − 0.06 and − 0.10 eV (Fig. S16 and S17), respectively, implying the relatively weaker interaction (physical adsorption) between O_2 and COF. The optimized structures of the COF–O_2 (COF–OOH) species show that the O—O bond in Py-TD-COF-NH is elongated to 1.36 Å (1.49 Å) relative to 1.25 Å (1.36 Å) in Py-TD-COF. It is noted that the O—O bond length in Py-TD-COF–O_2 is very close to the bond length of 1.23 Å in gas, which further proves the relatively weaker interaction of Py-TD-COF with O_2. The O-O elongation in Py-TD-COF-NH might be ascribed to the directed H-bonding interaction in the amine group. This result is similar with previous work that the H-bonding in the amine group could form a “pull effect” to elongate O—O bond in hydroperoxide [49]. Benefit from the effect of H-bonding, the elongated O—O bond with the trend of cleavage could facilitate the subsequent hydrogenation steps. This result is evidenced by the free energy diagrams for both $2e^-$ and $4e^-$ pathways at the potential of 1.23 V (Fig. 5c–d). Due to the H-bonding provided by the amine functionality in the backbone of Py-TD-COF-NH, a much lower ΔG_{*OOH} value is found on Py-TD-COF-NH (− 0.64 eV) than that on Py-TD-COF (0.40 eV). In addition, it is well accepted that an ideal catalyst for H_2O_2 synthesis needs to maximize the barrier for *OOH dissociation or reduction to *O and *OH (the intermediates of the $4e^-$ ORR pathway to H_2O) to achieve high selectivity. From the free energy diagrams, the barrier for *OOH dissociation to *OH on Py-TD-COF-NH is much reduced to 1.64 eV compared to that of Py-TD-COF (2.32 eV), showing the more thermodynamically favorable $2e^-$ ORR properties of Py-TD-COF over Py-TD-COF-NH. Moreover, it could also be evidenced by the energy differences between the two pivotal intermediates, H_2O_2 and *O. The ΔG_{*O}-ΔG_{H2O2} on Py-TD-COF (1.18 eV) is 0.67 eV lower than that of Py-TD-COF-NH (1.85 eV), implying that Py-TD-COF would exhibit higher selectivity for H_2O_2 production. To experimentally identify the critical intermediates during the H_2O_2 production, the operando FT-IR spectroscopy was performed using Py-TD-COF as the ORR catalyst (Fig. 5f). The adsorption band identified at 1062 cm^{-1} could be indexed to the stretching vibration of surface-adsorbed oxygen molecules [50]. More importantly, it is found that an adsorption band at 1259 cm^{-1} emerges in the FTIR spectrum and the intensity increases gradually as the potential decreases, showing the presence of vital intermediates

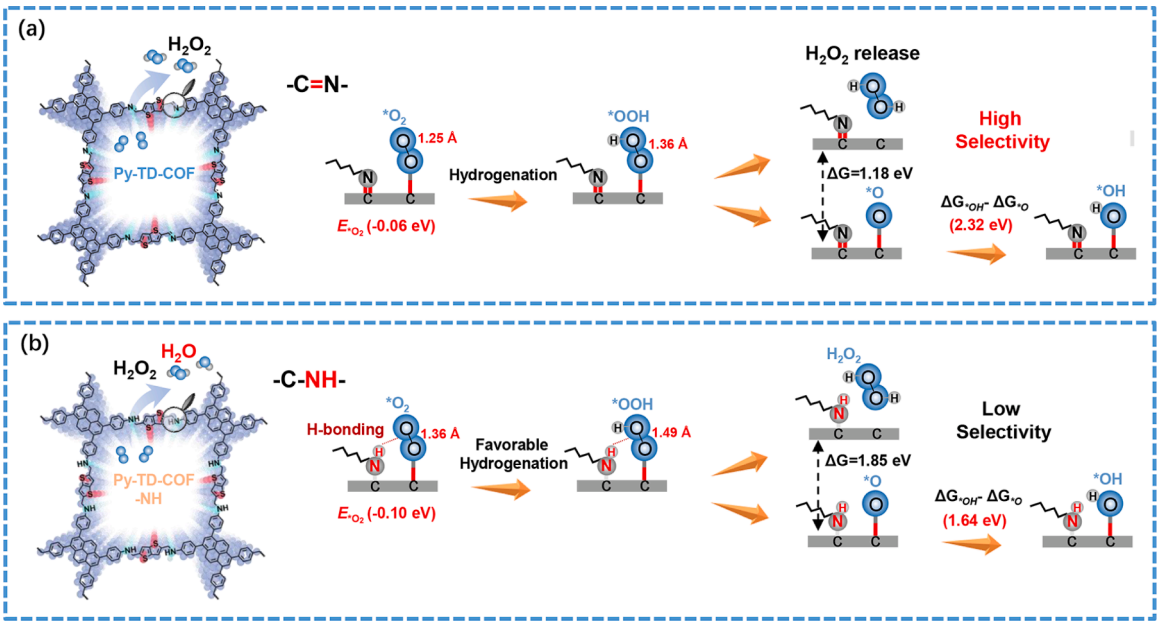

Fig. 6. Illustration of the possible reaction mechanism on (a) Py-TD-COF, (b) Py-TD-COF-NH.

during the ORR process. This vital intermediate can be ascribed to the superoxide species adsorbed on the surface of the catalyst (*OOH) [50, 51]. These results indicate that the key intermediates, adsorbed superoxide *OOH, are relatively stable on the active sites. It is not easy to be reduced, endowing the high H_2O_2 selectivity on Py-TD-COF during the ORR process, which is also in line with the experimental and theoretical calculation results.

3.4. $2e^-$ ORR mechanism on COFs

Based on the theoretical calculations and experiment results, possible ORR processes and mechanisms on Py-TD-COF and Py-TD-COF-NH are proposed. As presented in Fig. 6a, the donor-accepter property on Py-TD-COF enables proper activation of O_2, which results in the relatively weak adsorption of O_2 on the active site. The weak adsorption interaction would endow H_2O_2 release during the step of hydrogenation of $*O_2$ into *OOH, thus promoting the $2e^-$ ORR process. However, Py-TD-COF-NH shows relatively high activation of O_2 due to the matched electronic structure after the linkage transformation from imine to amine group. The relatively strong interaction of O_2 would lead to the stabilization of critical *OOH intermediates. Simultaneously, the interaction of hydrogen bonding in amine linkage can elongate the O—O bond of $*O_2$ and key intermediate *OOH, weakening the O—O bond. It could accelerate the subsequent hydrogenation step (Fig. 6b). Therefore, the resulting reduction of *OOH intermediate at a relatively low barrier becomes much easier than that on Py-TD-COF, leading to the partly O-O cleavage and an obvious decrease in H_2O_2 selectivity. In this regard, it is proposed that the relatively stronger activation of O_2 and potential H-bonding due to the amine functional groups close to the active sites are responsible for the low experimental selectivity to H_2O_2 in Py-TD-COF-NH.

4. Conclusion

In conclusion, we designed two kinds of COFs with different linkages and investigated their influence on the electrocatalytic ORR performance. The imine-linked Py-TD-COF, with typical donor-accepter property, shows a remarkable H_2O_2 selectivity of 80–92 % in the potential range of 0.2–0.7 V vs. RHE, while amine-linked Py-TD-COF-NH exhibits relatively low H_2O_2 selectivity of 50–61 % at the same potential wide. The theoretical calculation and experimental results revealed that the modulated electronic structure induced by the simple linkage transformation leads to the different activation abilities of O_2 on COFs. Moreover, directed H-bonding provided by amine linkage may elongate and weaken the O—O bond, facilitating the subsequent hydrogenation step. It is evidenced by the more downhill in free energy for *OOH reduction to *O on Py-TD-COF-NH. It is proposed that the relatively stronger activation of O_2 and potential H-bonding in amine linkage are responsible for the diminishment of H_2O_2 selectivity in Py-TD-COF-NH. The operando FT-IR spectroscopies further confirm the main $2e^-$ pathway during the ORR process on Py-TD-COF. This work well reveals the intrinsic correlation between linkages of COFs and electrocatalytic ORR behavior, which provides a guideline to design metal-free COF materials by linkage engineering for electrochemical oxygen reduction applications.

CRediT authorship contribution statement

Shaoda Huang: Conceptualization, Methodology, Formal analysis, Data curation, Writing – original draft. **Bingyan Zhang:** Formal analysis, Data curation. **Dongshuang Wu:** Validation, Investigation, Formal analysis. **Yifan Xu:** Formal analysis. **Hongyin Hu:** Formal analysis. **Fang Duan:** Validation, Investigation. **Han Zhu:** Validation, Investigation. **Mingliang Du:** Investigation, Supervision, Funding acquisition. **Shuanglong Lu:** Supervision, Project administration, Funding acquisition, Writing – review & editing.

Declaration of Competing Interest

The authors declare that they have no known competing financial interests or personal relationships that could have appeared to influence the work reported in this paper.

Data Availability

Data will be made available on request.

Acknowledgments

The authors would like to thank the National Natural Science Foundation of China (NSFC) (52173201, 21905115) and the China Scholarship Council, the MOE & SAFEA, 111 Project (B13025), the

Fundamental Research Funds for the Central Universities (JUSRP622039) and Postgraduate Research & Practice Innovation Program of Jiangsu Province (KYCX22_2323). The authors would also like to thank the characterizations supported by Central Laboratory, School of Chemical and Material Engineering, Jiangnan University.

Appendix A. Supporting information

Supplementary data associated with this article can be found in the online version at doi:10.1016/j.apcatb.2023.123216.

References

[1] Y. Sun, L. Han, P. Strasser, A comparative perspective of electrochemical and photochemical approaches for catalytic H_2O_2 production, Chem. Soc. Rev. 49 (2020) 6605–6631.
[2] S.C. Perry, D. Pangotra, L. Vieira, L.-I. Csepei, V. Sieber, L. Wang, C. Ponce de León, F.C. Walsh, Electrochemical synthesis of hydrogen peroxide from water and oxygen, Nat. Rev. Chem. 3 (2019) 442–458.
[3] Q. Yang, W. Xu, S. Gong, G. Zheng, Z. Tian, Y. Wen, L. Peng, L. Zhang, Z. Lu, L. Chen, Atomically dispersed lewis acid sites boost 2-electron oxygen reduction activity of carbon-based catalysts, Nat. Commun. 11 (2020) 5478.
[4] C. Tang, Y. Zheng, M. Jaroniec, S.-Z. Qiao, Electrocatalytic refinery for sustainable production of fuels and chemicals, Angew. Chem. Int. Ed. 60 (2021) 19572–19590.
[5] H.W. Kim, M.B. Ross, N. Kornienko, L. Zhang, J. Guo, P. Yang, B.D. McCloskey, Efficient hydrogen peroxide generation using reduced graphene oxide-based oxygen reduction electrocatalysts, Nat. Catal. 1 (2018) 282–290.
[6] M. Wang, N. Zhang, Y. Feng, Z. Hu, Q. Shao, X. Huang, Partially pyrolyzed binary metal-organic framework nanosheets for efficient electrochemical hydrogen peroxide synthesis, Angew. Chem. Int. Ed. 59 (2020) 14373–14377.
[7] J.M. Campos-Martin, G. Blanco-Brieva, J.L.G. Fierro, Hydrogen peroxide synthesis: an outlook beyond the anthraquinone process, Angew. Chem. Int. Ed. 45 (2006) 6962–6984.
[8] R. Ciriminna, L. Albanese, F. Meneguzzo, M. Pagliaro, Hydrogen peroxide: a key chemical for today's sustainable development, ChemSusChem 9 (2016) 3374–3381.
[9] J.K. Edwards, S.J. Freakley, R.J. Lewis, J.C. Pritchard, G.J. Hutchings, Advances in the direct synthesis of hydrogen peroxide from hydrogen and oxygen, Catal. Today 248 (2015) 3–9.
[10] Y. Jiang, P. Ni, C. Chen, Y. Lu, P. Yang, B. Kong, A. Fisher, X. Wang, Selective electrochemical H_2O_2 production through two-electron oxygen electrochemistry, Adv. Energy Mater. 8 (2018), 1801909.
[11] N. Wang, S. Ma, P. Zuo, J. Duan, B. Hou, Recent progress of electrochemical production of hydrogen peroxide by two-electron oxygen reduction reaction, Adv. Sci. 8 (2021), 2100076.
[12] Y. Bu, Y. Wang, G.-F. Han, Y. Zhao, X. Ge, F. Li, Z. Zhang, Q. Zhong, J.-B. Baek, Carbon-based electrocatalysts for efficient hydrogen peroxide production, Adv. Mater. 33 (2021), 2103266.
[13] Y. Wang, G.I.N. Waterhouse, L. Shang, T. Zhang, Electrocatalytic oxygen reduction to hydrogen peroxide: from homogeneous to heterogeneous electrocatalysis, Adv. Energy Mater. 11 (2021), 2003323.
[14] X. Yang, Y. Zeng, W. Alnoush, Y. Hou, D. Higgins, G. Wu, Tuning two-electron oxygen-reduction pathways for H_2O_2 electrosynthesis via engineering atomically dispersed single metal site catalysts, Adv. Mater. 34 (2022), 2107954.
[15] J.S. Jirkovský, I. Panas, E. Ahlberg, M. Halasa, S. Romani, D.J. Schiffrin, Single atom hot-spots at Au–Pd nanoalloys for electrocatalytic H_2O_2 production, J. Am. Chem. Soc. 133 (2011) 19432–19441.
[16] R. Shen, W. Chen, Q. Peng, S. Lu, L. Zheng, X. Cao, Y. Wang, W. Zhu, J. Zhang, Z. Zhuang, C. Chen, D. Wang, Y. Li, High-concentration single atomic Pt sites on hollow CuS_x for selective O_2 reduction to H_2O_2 in acid solution, Chem 5 (2019) 2099–2110.
[17] X. Zhang, C. Wang, K. Chen, A.H. Clark, R. Hübner, J. Zhan, L. Zhang, A. Eychmüller, B. Cai, Optimizing the Pd sites in pure metallic aerogels for efficient electrocatalytic H_2O_2 production, Adv. Mater. 35 (2023), 2211512.
[18] S. Geng, Y. Ji, S. Yang, J. Su, Z. Hu, T.-S. Chan, H. Yu, Y. Li, Y.-Y. Chin, X. Huang, Q. Shao, Phosphorus optimized metastable hexagonal-close-packed phase nickel for efficient hydrogen peroxide production in neutral media, Adv. Funct. Mater. (2023), 2300636.
[19] C. Zhang, L. Yuan, C. Liu, Z. Li, Y. Zou, X. Zhang, Y. Zhang, Z. Zhang, G. Wei, C. Yu, Crystal engineering enables cobalt-based-metal–organic frameworks as high-performance electrocatalysts for H_2O_2 production, J. Am. Chem. Soc. 145 (2023) 7791–7799.
[20] Y.-H. Wang, Z.K. Goldsmith, P.E. Schneider, C.W. Anson, J.B. Gerken, S. Ghosh, S. Hammes-Schiffer, S.S. Stahl, Kinetic and mechanistic characterization of low-overpotential, H_2O_2-selective reduction of O_2 catalyzed by N_2O_2-ligated cobalt complexes, J. Am. Chem. Soc. 140 (2018) 10890–10899.
[21] J. Li, X. Jing, Q. Li, S. Li, X. Gao, X. Feng, B. Wang, Bulk COFs and COF nanosheets for electrochemical energy storage and conversion, Chem. Soc. Rev. 49 (2020) 3565–3604.
[22] R.-R. Liang, S.-Y. Jiang, R.-H. A, X. Zhao, Two-dimensional covalent organic frameworks with hierarchical porosity, Chem. Soc. Rev. 49 (2020) 3920–3951.
[23] K. Geng, T. He, R. Liu, S. Dalapati, K.T. Tan, Z. Li, S. Tao, Y. Gong, Q. Jiang, D. Jiang, Covalent organic frameworks: design, synthesis, and functions, Chem. Rev. 120 (2020) 8814–8933.
[24] M.S. Lohse, T. Bein, Covalent organic frameworks: structures, synthesis, and applications, Adv. Funct. Mater. 28 (2018), 1705553.
[25] Y. Yusran, Q. Fang, V. Valtchev, Electroactive covalent organic frameworks: design, synthesis, and applications, Adv. Mater. 32 (2020), 2002038.
[26] S. Yang, Q. Cheng, J. Mao, Q. Xu, Y. Zhang, Y. Guo, T. Tan, W. Luo, H. Yang, Z. Jiang, Rational design of edges of covalent organic networks for catalyzing hydrogen peroxide production, Appl. Catal. B 298 (2021), 120605.
[27] X. Xu, Y. Gao, Q. Yang, T. Liang, B. Luo, D. Kong, X. Li, L. Zhi, B. Wang, Regulating the activity of intrinsic sites in covalent organic frameworks by introducing electro-withdrawing groups towards highly selective H_2O_2 electrosynthesis, Nano Today 49 (2023), 101792.
[28] X. Zhao, P. Pachfule, A. Thomas, Covalent organic frameworks (COFs) for electrochemical applications, Chem. Soc. Rev. 50 (2021) 6871–6913.
[29] X. Cui, S. Lei, A.C. Wang, L. Gao, Q. Zhang, Y. Yang, Z. Lin, Emerging covalent organic frameworks tailored materials for electrocatalysis, Nano Energy 70 (2020), 104525.
[30] X. Yan, B. Wang, J. Ren, X. Long, D.J.A.C. Yang, An unsaturated bond strategy to regulate active centers of metal-free covalent organic frameworks for efficient oxygen reduction, Angew. Chem. Int. Ed. 134 (2022), e202209583.
[31] R. Bao, Z. Xiang, Z. Qiao, Y. Yang, Y. Zhang, D. Cao, C. Wang, Designing thiophene-enriched fully conjugated 3D covalent organic framework as metal-free oxygen reduction catalyst for hydrogen fuel cells, Angew. Chem. Int. Ed. 135 (2023), e202216751.
[32] Z. You, B. Wang, Z. Zhao, Q. Zhang, W. Song, C. Zhang, X. Long, Y. Xia, Metal-free carbon-based covalent organic frameworks with heteroatom-free units boost efficient oxygen reduction, Adv. Mater. 35 (2023), 2209129.
[33] S. Huang, S. Lu, Y. Hu, Y. Cao, Y. Li, F. Duan, H. Zhu, Y. Jin, M. Du, W. Zhang, Covalent organic frameworks with molecularly electronic modulation as metal-free electrocatalysts for efficient hydrogen peroxide production, Small Struct. (2023), 2200387.
[34] X. Li, S. Yang, M. Liu, X. Yang, Q. Xu, G. Zeng, Z. Jiang, Catalytic linkage engineering of covalent organic frameworks for the oxygen reduction reaction, Angew. Chem. Int. Ed. (2023), e202304356.
[35] Z. Yang, J. Liu, Y. Li, G. Zhang, G. Xing, L.J.A.C. Chen, Arylamine-linked 2D covalent organic frameworks for efficient pseudocapacitive energy storage, Angew. Chem. Int. Ed. 133 (2021) 20922–20927.
[36] M. Liu, S. Yang, X. Yang, C.-X. Cui, G. Liu, X. Li, J. He, G.Z. Chen, Q. Xu, G. Zeng, Post-synthetic modification of covalent organic frameworks for CO_2 electroreduction, Nat. Commun. 14 (2023) 3800.
[37] H. Wang, C. Qian, J. Liu, Y. Zeng, D. Wang, W. Zhou, L. Gu, H. Wu, G. Liu, Y. Zhao, Integrating suitable linkage of covalent organic frameworks into covalently bridged inorganic/organic hybrids toward efficient photocatalysis, J. Am. Chem. Soc. 142 (2020) 4862–4871.
[38] H. Liu, J. Chu, Z. Yin, X. Cai, L. Zhuang, H. Deng, Covalent organic frameworks linked by amine bonding for concerted electrochemical reduction of CO_2, Chem 4 (2018) 1696–1709.
[39] S. An, X. Li, S. Shang, T. Xu, S. Yang, C.X. Cui, C. Peng, H. Liu, Q. Xu, Z. Jiang, J. Hu, One-dimensional covalent organic frameworks for the 2e(-) oxygen reduction reaction, Angew. Chem. Int. Ed. 62 (2023), e202218742.
[40] L. Ascherl, E.W. Evans, M. Hennemann, D. Di Nuzzo, A.G. Hufnagel, M. Beetz, R. H. Friend, T. Clark, T. Bein, F. Auras, Solvatochromic covalent organic frameworks, Nat. Commun. 9 (2018) 3802.
[41] J. Zhao, J. Ren, G. Zhang, Z. Zhao, S. Liu, W. Zhang, L. Chen, Donor-acceptor type covalent organic frameworks, Chem. Eur. J. 27 (2021) 10781–10797.
[42] M. Zhang, Y. Li, W. Yuan, X. Guo, C. Bai, Y. Zou, H. Long, Y. Qi, S. Li, G. Tao, C. Xia, L. Ma, Construction of flexible amine-linked covalent organic frameworks by catalysis and reduction of formic acid via the eschweiler–clarke reaction, Angew. Chem. Int. Ed. 60 (2021) 12396–12405.
[43] G.-F. Han, F. Li, W. Zou, M. Karamad, J.-P. Jeon, S.-W. Kim, S.-J. Kim, Y. Bu, Z. Fu, Y. Lu, S. Siahrostami, J.-B. Baek, Building and identifying highly active oxygenated groups in carbon materials for oxygen reduction to H_2O_2, Nat. Commun. 11 (2020) 2209.
[44] K. Dong, J. Liang, Y. Wang, Z. Xu, Q. Liu, Y. Luo, T. Li, L. Li, X. Shi, A.M. Asiri, Q. Li, D. Ma, X. Sun, Honeycomb carbon nanofibers: a superhydrophilic O_2-entrapping electrocatalyst enables ultrahigh mass activity for the two-electron oxygen reduction reaction, Angew. Chem. Int. Ed. 60 (2021) 10583–10587.
[45] A.N.E.S.M. Kozlov, F. Viñes, F. Illas, Electronic-structure-based chemical descriptors:(in) dependence on self-interaction and Hartree-Fock exchange, Phys. Rev. B 54 (1996) 11169–11186.
[46] B. Liu, X. Wang, J.L. Xu, D. Tian, R.Y. Chen, J. Xu, X.H. Buab, Electronic supporting information (ESI), Phys. Rev. B 49 (1994) 16223–16233.
[47] S. Grimme, J. Antony, S. Ehrlich, H. Krieg, A consistent and accurate ab initio parametrization of density functional dispersion correction (DFT-D) for the 94 elements H-Pu, J. Chem. Phys. 132 (2010), 154104.
[48] J.K. Nørskov, J. Rossmeisl, A. Logadottir, L. Lindqvist, J.R. Kitchin, T. Bligaard, H. Jónsson, Origin of the overpotential for oxygen reduction at a fuel-cell cathode, J. Phys. Chem. B 108 (2004) 17886–17892.

[49] A. Ghatak, S. Bhunia, A. Dey, Effect of pendant distal residues on the rate and selectivity of electrochemical oxygen reduction reaction catalyzed by iron porphyrin complexes, ACS Catal. 10 (2020) 13136–13148.
[50] S. Mondal, D. Bagchi, M. Riyaz, S. Sarkar, A.K. Singh, C.P. Vinod, S.C. Peter, In situ mechanistic insights for the oxygen reduction reaction in chemically modulated ordered intermetallic catalyst promoting complete electron transfer, J. Am. Chem. Soc. 144 (2022) 11859–11869.
[51] C. Tang, L. Chen, H. Li, L. Li, Y. Jiao, Y. Zheng, H. Xu, K. Davey, S.-Z. Qiao, Tailoring acidic oxygen reduction selectivity on single-atom catalysts via modification of first and second coordination spheres, J. Am. Chem. Soc. 143 (2021) 7819–7827.